

On the stability and maximum mass of differentially rotating relativistic stars

Lukas R. Weih¹ , Elias R. Most¹ and Luciano Rezzolla^{1,2}

¹*Institut für Theoretische Physik, Goethe Universität Frankfurt, Max-von-Laue-Str.1, 60438 Frankfurt am Main, Germany*

²*Frankfurt Institute for Advanced Studies, Ruth-Moufang-Str. 1, 60438 Frankfurt am Main, Germany*

13 March 2022

ABSTRACT

The stability properties of rotating relativistic stars against prompt gravitational collapse to a black hole are rather well understood for uniformly rotating models. This is not the case for differentially rotating neutron stars, which are expected to be produced in catastrophic events such as the merger of binary system of neutron stars or the collapse of a massive stellar core. We consider sequences of differentially rotating equilibrium models using the j -constant law and by combining them with their dynamical evolution, we show that a sufficient stability criterion for differentially rotating neutron stars exists similar to the one of their uniformly rotating counterparts. Namely: along a sequence of constant angular momentum, a dynamical instability sets in for central rest-mass densities slightly below the one of the equilibrium solution at the turning point. In addition, following Breu & Rezzolla (2016), we show that “quasi-universal” relations can be found when calculating the turning-point mass. In turn, this allows us to compute the maximum mass allowed by differential rotation, $M_{\text{max,dr}}$, in terms of the maximum mass of the nonrotating configuration, M_{TOV} , finding that $M_{\text{max,dr}} \simeq (1.54 \pm 0.05) M_{\text{TOV}}$ for all the equations of state we have considered.

Key words: stars: neutron – stars: rotation – methods: numerical – instabilities

1 INTRODUCTION

Simulations of binary neutron-star mergers have shown that the merger remnant is a differentially rotating neutron star [see Baiotti & Rezzolla (2017) for a recent review]. Depending on the total mass, mass ratio and equation of state (EOS) of the binary, the remnant may be a hypermassive neutron star (HMNS) and collapse to a black hole on a timescale $\lesssim 1$ s, or be a long-lived supramassive neutron star, or even a stable neutron star. The possible outcome has important implications on the gravitational-wave signal of such a merger, whose detection could be imminent. While the simulations of merging binaries are computationally expensive, an equilibrium solution of a differentially rotating neutron star is a good and inexpensive approximation for certain types of problems. Thus, a lot of studies have been dedicated to such solutions, either for their equilibrium (Baumgarte et al. 2000; Lyford et al. 2003; Ansorg et al. 2009; Gondek-Rosińska et al. 2017; Studzińska et al. 2016) or for their dynamics (Duez et al. 2006; Giacomazzo et al. 2011). Following these studies, we here use the “ j -constant” law to model differential rotation (see also Sec. 2.1); while commonly used, this rotation law is not a good approximation for the differentially rotating object produced in binary neutron-star mergers [see, e.g., Kastaun & Galeazzi (2015); Hanauske et al. (2017)], but may

be considered as a first step towards studying the stability properties of differentially rotating neutron stars.

The stability of neutron stars is a classical problem in general relativity and one of its most important results is the so-called “turning-point criterion” by Friedman et al. (1988). It states that along a sequence of nonrotating relativistic stars, secular instability sets in at the maximum of this sequence, i.e., at the turning point. On the other hand, Takami et al. (2011) found that for uniformly rotating stars this is just a sufficient, not a necessary criterion. The onset of dynamical instability is instead marked by the neutral-stability line, i.e., where the eigenfrequency of the fundamental mode of oscillation vanishes. The neutral-stability line and the turning-point line coincide for nonrotating neutron stars, but their difference grows with increasing angular momentum (Takami et al. 2011).

We here analyse the stability of differentially rotating neutron stars by carefully choosing 53 equilibrium models along sequences of constant angular momentum close to their respective turning points and evolving them dynamically in full general relativity. The choice of models close to their turning points is based on the conjecture that a neutral-stability line as found in Takami et al. (2011) also exists for differentially rotating neutron stars. Arguing that the neutral-stability line is reasonably close to the turning points, the latter are routinely used to find the stability limit not just for uniformly (Baiotti et al. 2005), but also for differentially rotating neutron stars (Bauswein & Stergioulas 2017; Kaplan

* E-mail: weih@th.physik.uni-frankfurt.de

2014). Using fully general-relativistic numerical simulations we show that this assumption is indeed correct and the turning-point line can be used as an approximation for finding the threshold mass for prompt collapse to a black hole. Our results apply in particular to the class of solutions of “type A”, as classified by [Ansorg et al. \(2009\)](#). These differentially rotating stars always have the maximum of the rest-mass density at the stellar center, are spheroidal, and possess a mass-shedding limit. When considering the properties of the remnant of binary neutron-star merger simulations, this class of solutions appears to be the most realistic one.

In addition, we present a “quasi-universal” relation that allows us to determine the turning-point mass of differentially rotating neutron stars independently of the underlying EOS. This relation is an extension to what was found by [Breu & Rezzolla \(2016\)](#) for uniformly rotating stars and is in agreement with what was recently presented by [Bozzola et al. \(2017\)](#). More importantly, using this relation, we can estimate the maximum mass allowed by differential rotation, $M_{\text{max, dr}}$, in terms of the maximum mass of the nonrotating configuration, M_{TOV} . We find that $M_{\text{max, dr}} \simeq (1.54 \pm 0.05) M_{\text{TOV}}$ for all the EOSs considered.

The organization of the paper is as follows. In [Sec. 2.1](#) we discuss the equilibrium models, while the numerical setup of the numerical evolution is described in [Sec. 2.2](#), followed by the presentation of the results in [Sec. 3](#). The quasi-universal relation for the maximum mass is discussed in [Sec. 4](#), while our results are summarised in [Sec. 5](#). Unless stated differently, we use units in which $c = G = M_{\odot} = 1$ and call simply “mass” the gravitational mass.

2 NUMERICAL SETUP AND INITIAL DATA

2.1 Initial Data

The initial data represents axisymmetric models of self-gravitating matter configurations in equilibrium and is computed numerically making use of the RNS code ([Stergioulas & Friedman 1995](#)), which solves the Einstein equations together with the equation of hydro-stationary equilibrium. Differential rotation is then introduced via a rotation-law function $F(\Omega)$ that depends on the angular velocity Ω only and determines the star’s rotation profile. For our equilibrium models we chose the commonly used j -constant law

$$F(\Omega) = A^2(\Omega_c - \Omega), \quad (1)$$

where Ω_c is the central angular velocity and A is a free parameter with dimension length that determines the degree of differential rotation. We adopt the parametrization $\tilde{A} := r_e/A$ with r_e being the equatorial coordinate radius¹. In this way, the limit of uniform rotation is obtained for $\tilde{A} = 0$, while higher values of \tilde{A} lead to higher degrees of differential rotation, i.e., steeper rotation profiles. Another consequence of differential rotation is that for higher values of \tilde{A} , higher angular momenta J can be reached, which, in turn, shifts the mass-shedding limit to higher masses. This is shown in [Fig. 1](#), which reports sequences of nonrotating models ($\Omega = 0$), together with the mass-shedding limits of uniformly rotating models ($\Omega_{\text{K};0}$), and of differentially rotating models with different degrees of differential rotation ($\Omega_{\text{K};0.20} - \Omega_{\text{K};0.57}$).

The initial data for the dynamical evolution is modeled with a polytropic EOS with $\Gamma = 2.0$ and $K = 100$ ([Rezzolla & Zanotti 2013](#)) and we compute a wide range of models by specifying the values for \tilde{A} , the central rest-mass density ρ_c , and the ratio of polar

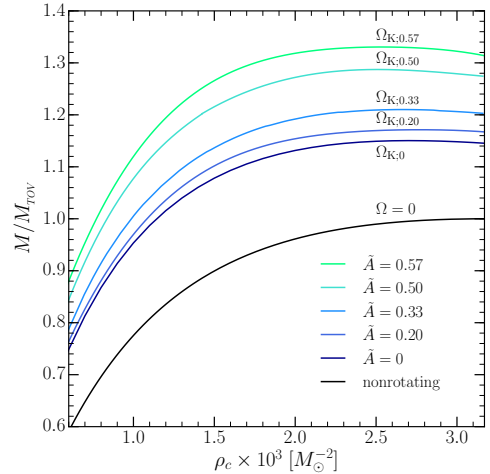


Figure 1. Generic sequences of equilibrium solutions with polytropic EOS: nonrotating models ($\Omega = 0$), mass-shedding limits of uniformly rotating models ($\Omega_{\text{K};0}$), and mass-shedding limits of differentially rotating models with different degrees of differential rotation ($\Omega_{\text{K};0.20} - \Omega_{\text{K};0.57}$).

to equatorial radius. We then arrange these models as sequences of constant angular momentum² parametrized by ρ_c . Such sequences are shown in [Fig. 2](#), which also reports the location of the initial data used for the dynamical evolution with open circles. On the other hand, for the quasi-universal relation presented in [Sec. 4](#) the equilibria are computed in the same way, but with eight nuclear-physics cold EOSs in tabulated form: DD2, NL3, SLy, SKa, SK272, SK255, SFHX, and SFHO [see [Baiotti & Rezzolla \(2017\)](#) for a list of references to these EOSs which we omit for compactness here]. Note that we have fixed the electron fraction assuming beta equilibrium and the temperature to be the lowest table entry for hot EOS. We point out that all the EOS used here are compatible with the $2M_{\odot}$ constraint of nonrotating neutron stars ([Demorest et al. 2010](#); [Antoniadis et al. 2013](#)).

2.2 Numerical Setup

From the initial data the necessary quantities of the 3+1 formalism are computed and mapped on a Cartesian grid. In order to extend the grid and increase the resolution within the star fixed mesh refinement is used, which is provided by the Carpet driver ([Schnetter et al. 2004](#)). Two refinement levels are used with an inner grid resolution of $h_1 = 0.1 M_{\odot}$ (~ 148 m), and the outer grid with half that resolution. The results have been confirmed to be the qualitatively same when employing a higher resolution of $h_1 = 0.07 M_{\odot}$ (~ 100 m) and a lower resolution of $h_1 = 0.15 M_{\odot}$ (~ 220 m). The boundary of the inner level is placed at $12 M_{\odot}$ (~ 17.7 km) so that the star lies in all cases well within this inner region. The outer boundary is placed at twice that distance (it has been verified that the outer boundary at four times the inner one yields the same results). In order to save computation time the neutron star’s symmetry is exploited and a reflection symmetry across the $z = 0$ plane is adopted. The spacetime is evolved using the fourth-order finite-differencing code McLachlan ([Löffler et al. 2012](#)) and apparent horizons are computed by AHFinderDirect ([Thornburg 2004](#)). The McLachlan code solves the equations of the CCZ4

¹ Another commonly used parametrization is $\hat{A} := A/r_e = \tilde{A}^{-1}$.

² The variance of the angular momentum from a constant value is $\lesssim 1\%$.

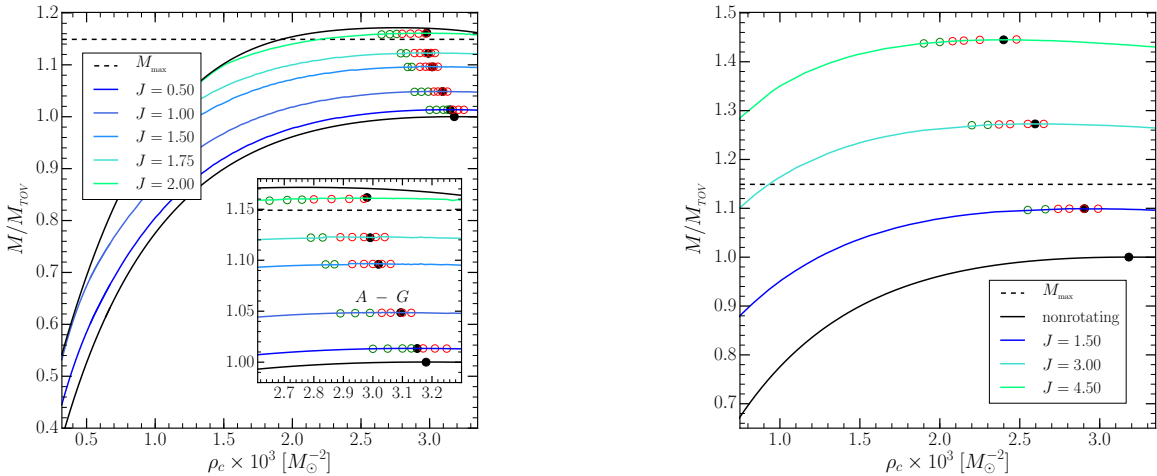


Figure 2. *Left panel:* Sequences of constant angular momentum for $\tilde{A} = 0.2$. The lower and upper black line refer to the nonrotating and mass-shedding sequences, i.e., $\Omega = 0$ and $\Omega_{K;0.20}$, respectively. Black filled circles denote the turning points, while the open circles mark the dynamically evolved models. The red circles, collapse on a dynamical timescale, while the green ones do not. Models *A-G* are labelled from left to right, while an horizontal dashed line marks the maximum mass of uniformly rotating models, M_{\max} . *Right panel:* Same as in the left panel, but for $\tilde{A} = 0.77$. Note that an overall mass shedding limit does not exist for this degree of differential rotation.

formulation (Alic et al. 2012) using the $1 + \log$ slicing condition for the lapse (Alcubierre et al. 2000) and the Gamma-driver condition for the shift (Alcubierre et al. 2001). On the other hand, the evolution of the hydrodynamic quantities is done by the high-order WhiskyTHC code (Radice & Rezzolla 2012; Radice et al. 2014b,a) employing an ideal-fluid EOS with $\gamma = 2$. It employs a fifth-order monotonicity preserving flux reconstruction (MP5) (Suresh & Huynh 1997) and is coupled to a third-order Runge-Kutta time integrator with a Courant factor of 0.15.

In principle, the truncation error of the initial data is sufficient to excite perturbations in the star and hence either quasi-normal mode oscillations or trigger the gravitational collapse (Baiotti et al. 2005). However, given an unstable equilibrium model, the properties of our truncation error always lead the star to migrate to the stable branch of solutions rather than collapsing to a black hole (Font et al. 2002). Because for models close to the turning point the solution on the unstable branch is very close in mass to the stable one, such a migration is almost indistinguishable from the actual oscillations of a stable star. A much clearer distinction is possible if the unstable models collapse, which can be ensured by decreasing the initial angular velocity according to

$$\delta\Omega(r, \theta, \phi) = \mathcal{A}\Omega(r, \theta, \phi), \quad (2)$$

where the amplitude \mathcal{A} of that relative perturbation has to be chosen carefully: a perturbation that is too strong might push a perfectly stable configuration over the stability limit and force it to collapse. To prevent this, the amplitude was gauged using results known for uniformly rotating stars and an analytic expression for the neutral-stability line for uniformly rotating neutron stars can be obtained by setting to zero Eq. (3) of Takami et al. (2011), i.e.,

$$\beta(\rho_c) = - \left(\sum_{n=0}^{n=5} a_n \rho_c^n \right) / \left(\sum_{n=0}^{n=5} b_n \rho_c^n \right), \quad (3)$$

where β is the ratio of kinetic to gravitational binding energy and the parameters a_n and b_n are given by Takami et al. (2011). Next, using the RNS code, we compute a sequence of uniformly rotating stars with constant angular momentum $J = 1.0$. The intersection of $\beta(\rho_c)$ for this sequence with Eq. (3) yields the location ρ_c^{crit}

of the stability limit for $J = 1.0$. We then select models of our sequence with central rest-mass densities that are slightly smaller and slightly larger than ρ_c^{crit} and set \mathcal{A} as the value for which the latter configuration collapses while the former does not. This value is then used to perturb the differentially rotating neutron stars.

3 NUMERICAL RESULTS AND ANALYSIS

In Fig. 3 the time evolution of the central rest-mass density ρ_c is shown for several models with $J = 1.0$ and $\tilde{A} = 0.2$ around the turning point of this sequence. The diverging curves clearly show the prompt collapse to a black hole and this is further confirmed by the detection of an apparent horizon. A collapsing model does so after $\sim 1 - 2$ ms and shows the same dynamics as was already observed for differentially rotating neutron stars by Giacomazzo et al. (2011). In contrast, the three models with the lowest densities do not collapse and show only small oscillations induced by the initial perturbation, which have been verified to vanish for unperturbed initial data and to correspond to the fundamental mode of oscillation (the frequency decreases near the threshold to stability).

Whether a model collapses or not should be independent of the kind of perturbation that is applied. Therefore, we additionally tested two models, i.e., one that was found to be stable and one unstable using the previous perturbation. We then evolved these models applying an inwards-directed radial perturbation of the form

$$\delta v_r(r, \theta, \phi) = \mathcal{B} |v(r, \theta, \phi)|, \quad (4)$$

where the absolute velocity is calculated as $|v| = \sqrt{g_{ij}v^i v^j}$ and the amplitude \mathcal{B} is gauged in the same way as was done for \mathcal{A} in (2). Although the collapse dynamics differs slightly depending on the perturbation, the fact whether a model collapses or not does not.

What can be seen in Fig. 3 looks qualitatively the same for all other sequences, i.e., the high-density models collapse while the low-density ones do not. Referring to Fig. 2, the stability properties of all the evolved models with $\tilde{A} = 0.20$ can be easily seen: black filled circles mark the turning points of the sequences of constant angular momentum, while red circles mark configurations that

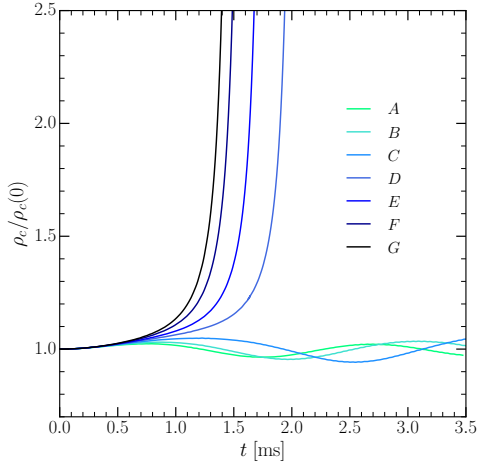


Figure 3. Evolution of the central rest-mass density normalised to its initial value. All models lie on the same sequence of constant angular momentum $J = 1.0$ and have a degree of differential rotation of $\tilde{A} = 0.2$ (cf., Fig. 2).

were found to collapse, and green circles mark the stable ones. The same analysis has been repeated for 18 models with a higher degree of differential rotation, i.e., $\tilde{A} = 0.77$. For this value no mass-shedding limit exists, because type-A stars cannot be found for higher J . The overall picture looks qualitatively similar to the one shown in Fig. 2, although the stability limit shifts even further to the low-density side of the turning point when J is increased.

Clearly, all the differentially rotating neutron stars to the high-density side of their respective turning point are unstable. As the turning point shifts to lower densities with increasing angular momentum, we can thus confirm what conjectured by Kaplan (2014): All the differentially rotating stars with central densities at or higher than the critical central density of a nonrotating model are unstable to gravitational collapse. While they conjectured this for all HMNSs, our results show it holds for all differentially rotating neutron stars of type A, including the non-hypermassive ones.

We should also note that the configurations on the low-density side of their respective turning point are not unconditionally stable. As is the case for uniformly rotating stars, the actual neutral-stability line is on the left of the turning-point line, so that stellar models that are on the left of the turning-point but on the right of the neutral-stability line may actually also be unstable [see Takami et al. (2011) for a discussion]. With increasing angular momentum the stability limit shifts to the low-density side of the turning point, but it is still reasonably close to the turning point, so that the approximation of taking the turning point as the stability limit is valid, at least for small values of J .

The models in Fig. 2 above the horizontal dashed line are HMNSs but have the same overall behavior as the non-hypermassive ones. It appears, therefore that the assumption that all HMNSs are dynamically unstable is not justified. However, HMNSs might still be secularly unstable and pass the neutral-stability line after redistributing their angular momentum.

4 MAXIMUM MASS AND UNIVERSAL RELATIONS

Figure 4 shows the normalised turning-point mass $M_{\max, \text{dr}}$ as a function of the normalised dimensionless angular momentum j/j_{\max} , for all of the eight cold tabulated EOSs considered. Here, $j := J/M^2$ and j_{\max} is instead the highest specific angular mo-

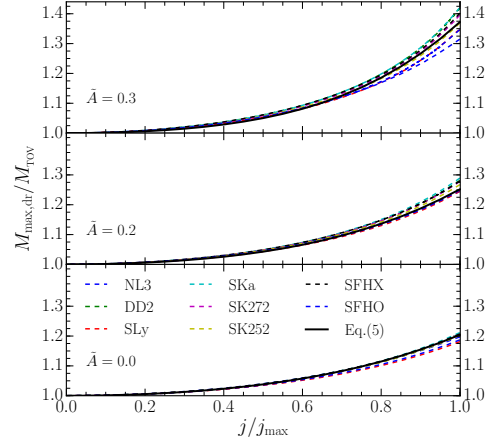


Figure 4. Normalised turning-point mass over normalised dimensionless angular momentum for eight different EOSs. The three panels correspond to three different degrees of differential rotation and the best-fitting functions are shown as thick solid black lines.

mentum which is at the mass-shedding limit in the case of uniform rotation, but not for $\tilde{A} > 0$. Lines of the same type are collected in three bundles – each consisting of eight coloured curves (one for each EOS) – corresponding to three representative values of \tilde{A} . The bundle in the lower panel corresponds to $\tilde{A} = 0$, hence to uniform rotation and should therefore be compared with the right panel of Fig. 1 in Breu & Rezzolla (2016). Figure 4 clearly highlights that the turning-point mass increases with growing j/j_{\max} in a quasi-universal manner, i.e., in a way that is almost insensitive to the EOS. As discussed by Breu & Rezzolla (2016), in the case of uniform rotation (i.e., $\tilde{A} = 0$), the turning-point mass reaches a maximum at $M_{\max} \simeq 1.2 M_{\text{TOV}}$. Our results show that this general behaviour remains the same also for non-zero values of \tilde{A} , as is evident from the two upper panels of Fig. 4 that refer to differentially rotating models. As done by Breu & Rezzolla (2016) we can now obtain corresponding fits, reported with thick lines of the same type and have the form

$$\frac{M_{\max, \text{dr}}(j, \tilde{A})}{M_{\text{TOV}}} = 1 + a_1(\tilde{A}) \left(\frac{j}{j_{\max}} \right)^2 + a_2(\tilde{A}) \left(\frac{j}{j_{\max}} \right)^4. \quad (5)$$

Because $M_{\max, \text{dr}}$ is a function of both j and \tilde{A} , the fitting parameters a_1 and a_2 are not constant, as in Breu & Rezzolla (2016), but depend now on the degree of differential rotation via \tilde{A} , with $a_1 = 0.13, 0.14, 0.14$ and $a_2 = 0.07, 0.11, 0.23$ for $\tilde{A} = 0, 0.2, 0.3$, respectively, and with relative variances that are $\lesssim 10\%$. We can collect the maximum mass $M_{\max, \text{dr}}(\tilde{A})$ found at $j/j_{\max} = 1$ for all of the eight EOSs and study its behaviour when \tilde{A} varies in the range $[0, \tilde{A}_{\max}]$, where \tilde{A}_{\max} is the maximum degree of differential rotation for which a mass-shedding limit can still be found, and which obviously depends on the EOS³. Using this procedure we are then able to concentrate on models that have the largest possible specific angular momentum and study how the maximum mass changes as function of \tilde{A} . Interestingly, we find a quasi-universal behaviour also in this case, which we model as

$$\frac{M_{\max, \text{dr}}(j_{\max}, \tilde{A})}{M_{\text{TOV}}} = 1.2 + b_1 \left(\frac{\tilde{A}}{\tilde{A}_{\max}} \right)^2 + b_2 \left(\frac{\tilde{A}}{\tilde{A}_{\max}} \right)^4, \quad (6)$$

³ We note that stars of “type C” in the classification of Ansorg et al. (2009) do not possess a mass-shedding limit and hence a value for \tilde{A}_{\max} .

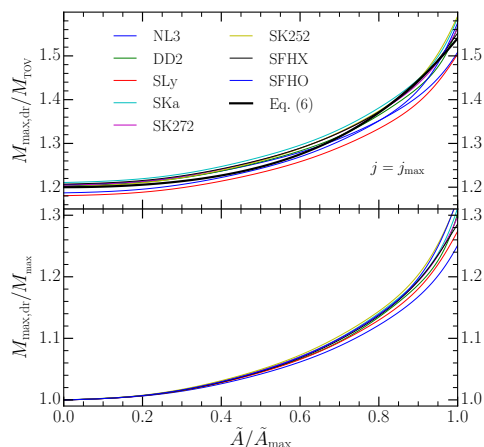


Figure 5. Maximum mass as a function of the normalised degree of differential rotation. In the upper panel the data is compared to the fit (6), while the lower panel further highlights the universal behavior by normalising the mass to the highest value obtained for uniform rotation, M_{\max} .

where $b_1 = 0.135$ and $b_2 = 0.206$. The global behaviour of the fitting function (5) for the quantity $M_{\max, \text{dr}}(\tilde{A})$ is shown in Fig. 5. Using (6) for $\tilde{A} = \tilde{A}_{\max}$, we then find “absolute” maximum mass (i.e., the maximum of the maxima) for a star in differential rotation of type A to be $M_{\max, \text{dr}} \simeq (1.54 \pm 0.05) M_{\text{TOV}}$, where the error estimate results from considering the largest error in our fits.

Before concluding this section we note that a universal relation between the turning-point mass and the angular momentum was reported recently also by Bozzola et al. (2017). The relation proposed in Eq. (13c) of Bozzola et al. (2017), however, does not allow to calculate masses larger than $M_{\max, \text{dr}} \simeq 1.2 M_{\text{TOV}}$, because the data used for determining the best-fitting function was limited to $J \in [0, 7]$ or, equivalently, $J/M_{\text{TOV}}^2 \in [0, 0.7]$. As a result, the fit deviates for neutron stars with higher J , as can be seen from Fig. 6. Of course, it is possible to repeat the fit in Eq. (13c) of Bozzola et al. (2017) by increasing the range for J , but this would then depend on the specific EOS, since different EOSs have different J_{\max} . Our analysis instead uses dimensionless quantities, i.e., j/j_{\max} , and so does not introduce arbitrary mass scales.

5 CONCLUSION

We have computed a large number of equilibrium models of differentially rotating relativistic stars of type A in the classification of Ansong et al. (2009), and evolved selected models along sequences of constant angular momentum and for two representative degrees of differential rotation. In this way, we have shown that the neutral-stability line that marks the onset of dynamical instability for uniformly rotating neutron stars can be extended also to differentially rotating ones. In turn, this indicates that all the rotating stars on the high-density side of the turning point on sequences of constant angular momentum are unstable solutions. Furthermore, because the neutral-stability limit is sufficiently close to the turning points, the turning-point criterion remains a reasonable first approximation to mark dynamically unstable models, at least for small values of J .

Following Breu & Rezzolla (2016), we have also shown that “quasi-universal” relations can be found for the turning-point mass, through which we compute the maximum mass allowed by differential rotation as $M_{\max, \text{dr}} \simeq (1.54 \pm 0.05) M_{\text{TOV}}$, with M_{TOV}

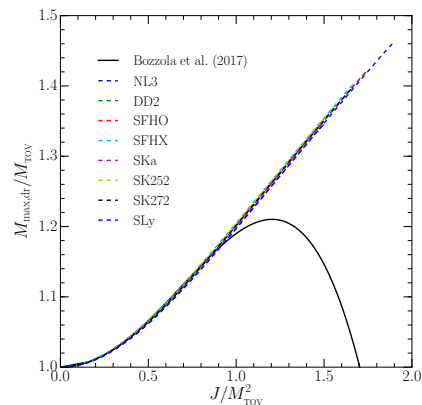


Figure 6. Normalised mass over J/M_{TOV}^2 . Shown is the data for eight EOSs and the comparison with expression (13c) by Bozzola et al. (2017).

the maximum nonrotating mass. Finally, we could confirm the validity of the universal relation derived for the one-parameter j -constant law by Bozzola et al. (2017), but also point out that such validity holds true only for a limited range of J .

As a final remark, we note that the analysis carried out here adopts the simple and commonly used law of differential rotation (1). However, binary neutron-star merger simulations have shown that the merged object has a rather different rotation profile, with a maximum off the centre [see, e.g., Kastaun & Galeazzi (2015); Hanauske et al. (2017)]. Recently, a new rotation law has been proposed that yields a rotation profile similar to the one from merger simulations (Uryu et al. 2017). The constant angular-momentum sequences calculated with this new law also exhibit turning points, suggesting that our results will hold qualitatively also with more realistic rotation profiles.

ACKNOWLEDGEMENTS

We thank G. Bozzola and C. Breu for useful discussions. This research is supported in part by the ERC synergy grant “Black-HoleCam: Imaging the Event Horizon of Black Holes” (Grant No. 610058), by “NewCompStar”, COST Action MP1304, by the LOEWE-Program in the Helmholtz International Center (HIC) for FAIR, by the European Union’s Horizon 2020 Research and Innovation Programme (Grant 671698) (call FETHPC-1-2014, project ExaHyPE). The simulations were performed on the SuperMUC cluster at the LRZ in Garching, on the LOEWE cluster in CSC in Frankfurt, on the HazelHen cluster at the HLRS in Stuttgart.

REFERENCES

- Alcubierre M., Brügmann B., Dramlitsch T., Font J. A., Papadopoulos P., Seidel E., Stergioulas N., Takahashi R., 2000, *Phys. Rev. D*, **62**, 044034
- Alcubierre M., Brügmann B., Pollney D., Seidel E., Takahashi R., 2001, *Phys. Rev. D*, **64**, 061501
- Alic D., Bona-Casas C., Bona C., Rezzolla L., Palenzuela C., 2012, *Phys. Rev. D*, **85**, 064040
- Ansong M., Gondek-Rosińska D., Villain L., 2009, *Mon. Not. R. Astron. Soc.*, **396**, 2359
- Antoniadis J., et al., 2013, *Science*, **340**, 448
- Baiotti L., Rezzolla L., 2017, *Rept. Prog. Phys.*, **80**, 096901
- Baiotti L., Hawke I., Montero P. J., Löffler F., Rezzolla L., Stergioulas N., Font J. A., Seidel E., 2005, *Phys. Rev. D*, **71**, 024035

6 *Weih, Most and Rezzolla*

- Baumgarte T. W., Shapiro S. L., Shibata M., 2000, *Astrophys. J.*, 528, L29
- Bauswein A., Stergioulas N., 2017, *Mon. Not. R. Astron. Soc.*, 471, 4956
- Bozzola G., Stergioulas N., Bauswein A., 2017, preprint, ([arXiv:1709.02787](https://arxiv.org/abs/1709.02787))
- Breu C., Rezzolla L., 2016, *Mon. Not. R. Astron. Soc.*, 459, 646
- Demorest P. B., Pennucci T., Ransom S. M., Roberts M. S. E., Hessels J. W. T., 2010, *Nature*, 467, 1081
- Duez M. D., Liu Y. T., Shapiro S. L., Shibata M., Stephens B. C., 2006, *Phys. Rev. D*, 73, 104015
- Font J. A., et al., 2002, *Phys. Rev. D*, 65, 084024
- Friedman J. L., Ipser J. R., Sorkin R. D., 1988, *Astrophys. J.*, 325, 722
- Giacomazzo B., Rezzolla L., Stergioulas N., 2011, *Phys. Rev. D*, 84, 024022
- Gondek-Rosińska D., Kowalska I., Villain L., Ansorg M., Kucaba M., 2017, *Astrophys. J.*, 837, 58
- Hanauske M., Takami K., Bovard L., Rezzolla L., Font J. A., Galeazzi F., Stöcker H., 2017, *Phys. Rev. D*,
- Kaplan J. D., 2014, PhD thesis, California Institute of Technology
- Kastaun W., Galeazzi F., 2015, *Phys. Rev. D*, 91, 064027
- Löffler F., et al., 2012, *Class. Quantum Grav.*, 29, 115001
- Lyford N. D., Baumgarte T. W., Shapiro S. L., 2003, *Astrophys. J.*, 583, 410
- Radice D., Rezzolla L., 2012, *Astron. Astrophys.*, 547, A26
- Radice D., Rezzolla L., Galeazzi F., 2014a, *Class. Quantum Grav.*, 31, 075012
- Radice D., Rezzolla L., Galeazzi F., 2014b, *Mon. Not. R. Astron. Soc. L.*, 437, L46
- Rezzolla L., Zanotti O., 2013, *Relativistic Hydrodynamics*. Oxford University Press, Oxford, UK, doi:10.1093/acprof:oso/9780198528906.001.0001
- Schnetter E., Hawley S. H., Hawke I., 2004, *Class. Quantum Grav.*, 21, 1465
- Stergioulas N., Friedman J. L., 1995, *Astrophys. J.*, 444, 306
- Studzińska A. M., Kucaba M., Gondek-Rosińska D., Villain L., Ansorg M., 2016, *Mon. Not. R. Astron. Soc.*, 463, 2667
- Suresh A., Huynh H. T., 1997, *Journal of Computational Physics*, 136, 83
- Takami K., Rezzolla L., Yoshida S., 2011, *Mon. Not. R. Astron. Soc.*, 416, L1
- Thornburg J., 2004, *Class. Quantum Grav.*, 21, 743
- Uryu K., Tsokaros A., Baiotti L., Galeazzi F., Taniguchi K., Yoshida S., 2017, preprint, ([arXiv:1709.02643](https://arxiv.org/abs/1709.02643))